Available online at www.sciencedirect.com
ScienceDirect
Journal of Power Sources 162 (2006) 985–991
JOURNAL OF POWER SOURCES
www.elsevier.com/locate/jpowsour

An investigation of convective transport in micro proton-exchange membrane fuel cells

A.S. Rawool [a], Sushanta K. Mitra [a,*], Jon G. Pharoah [b]

[a] *Department of Mechanical Engineering, Indian Institute of Technology Bombay, Mumbai 400076, India*
[b] *Department of Mechanical Engineering, Queen's-RMC Fuel Cell Research Center, Queen's University, Kingston, Ont., Canada*

Received 8 April 2006; accepted 24 July 2006
Available online 14 September 2006

Abstract

The flow phenomena in a serpentine microchannel segment attached to a porous transport layer in a micro proton-exchange membrane fuel cell is investigated. Due to the presence of a porous transport layer, the fluid flow for this configuration exhibits different characteristics compared with that through a simple serpentine channel. The pressure drop and friction factor variation in the channel is examined for various values of Reynolds number and radii of curvature. Also, the effect of variation of permeability is investigated. There are two modes of fluid transport in this geometry—one through the serpentine channel and other via the porous media. With increasing permeability, more fluid is convected through the porous transport layer.

Keywords: Porous; Bipolar plate; Numerical; Transport layer; Modeling; Proton-exchange membrane fuel cell

1. Introduction

Flow phenomena in large-scale fuel cells have been studied extensively during recent years. In a typical fuel cell configuration, fuel and oxidant are passed through a serpentine microchannel attached to a porous transport layer (PTL). While passing through the channel, the fluid diffuses through the PTL. The presence of a transport layer attached to the channel makes the flow characteristics significantly different from those through a simple channel. Pharoah [1] studied laminar flow through a serpentine channel with rectangular bends that was mounted on a permeable gas transport layer with isotropic and orthotropic permeabilities. Guvelioglu et al. [2] investigated multicomponent transport in proton exchange membrane fuel cells (PEMFCs) including electrochemical kinetics and water balance in the membrane. These authors also studied the effect of channel geometry on fuel cell performance. Ramousse et al. [3] investigated heat, mass and charge transfer in a single PEMFC. The independent solutions of heat and mass transfers in the cell were combined with a solution of coupled charge and mass transfers in the electrodes. Hontanona et al. [4] attempted the optimization of flow fields in fuel cells. In particular, the use of a grooved channel distributor and a porous material distributor in bipolar plates was evaluated.

Thus, it can be seen that the majority of the research work in this field has focused on species diffusion and electrochemistry in the porous transport layer. Also, these studies are related to flow through rectangular serpentine channels. There is a growing interest in using micro-fuel cells for portable applications. In these micro-fuel cells, the fuel channels are of micron cross-section and Reynolds numbers are typically very low (0.001–0.1). Hence, the flow through microchannels with serpentine bends needs to be investigated. The present authors have studied flow through serpentine microchannels with designed roughness in two dimensions [5] and three dimensions [6]. For serpentine flow fields in presence of a porous layer, the fluid has two different paths for convection from the inlet to the exit of the channel. One is through the serpentine microchannel; the second one is through the PTL. Depending on the permeability of the porous layer, some fluid may short-circuit through the PTL instead of passing through the microchannel. Thus, the convection in micro-fuel cell is characteristically different from simple microchannel flow, due to presence of a porous transport layer. To the best of authors' knowledge, no work is reported

* Corresponding author. Tel.: +91 22 2576 7513; fax: +91 22 2572 6875.
E-mail address: skmitra@me.iitb.ac.in (S.K. Mitra).

0378-7753/$ – see front matter © 2006 Elsevier B.V. All rights reserved.
doi:10.1016/j.jpowsour.2006.07.067

Nomenclature

D_h	hydraulic diameter of channel cross section (m)
f	friction factor
H_c	channel height (μm)
H_p	thickness of porous layer (μm)
K	permeability of porous transport layer (m^2)
L_c	length of straight segment of channel (μm)
P	pressure
R_c	radius of curvature of channel axis at bend (μm)
Re	Reynolds number
T	temperature of fluid (K)
u	velocity component in x-direction ($m\,s^{-1}$)
v	velocity component in y-direction ($m\,s^{-1}$)
w	velocity component in z-direction ($m\,s^{-1}$)
W_c	width of channel (μm)

Greek letters

ϵ	porosity of porous transport layer
μ	viscosity of fluid ($N\,s\,m^{-2}$)
τ	shear stress tensor

to understand such flows in micro-fuel cells. Hence, it is of interest to study convection in micro-PEMFCs.

2. Model for microchannel

The geometry of the flow channel in the micro-PEMFC under consideration is shown in Fig. 1. The channel has a square cross-section of $W_c = 100\ \mu m \times H_c = 100\ \mu m$. The length of the straight segment of channel is $L_c = 1000\ \mu m$. The radius of curvature of the microchannel at the bend is varied from 200 to 400 mm. The PTL, located below the micro-channel, has a thickness of $H_p = 40\ \mu m$. Such flow path configurations are commonly observed in fuel cells in which a number of serpentine channel segments in series act as a passage for the fuel and the oxidant. Usually, carbon cloth, carbon paper or Toray paper is employed as the PTL material. The pore sizes in such materials can range from submicrons to few microns. For mass transfer applications, such small pore sizes result in Knudsen diffusion, as discussed by Litster et al. [7]. Nevertheless, here it is assumed that the Brinkman–Forchheimer extension of the Darcy equation is valid for convection through the PTL.

3. Governing equations

The governing equations for the flow through the channel are the mass conservation and Navier–Stokes equations, which are given as:

$$\nabla(\rho V) = 0 \tag{1}$$

$$\rho V(\nabla \cdot V) = -\nabla P + \mu \nabla^2 V \tag{2}$$

where ρ is the density of fluid, which is air in this case; V the velocity; μ the viscosity; P the pressure. For the porous transport layer, the mass conservation and momentum conservation equations become, respectively:

$$\nabla(\epsilon \rho V) = 0 \tag{3}$$

$$\nabla(\epsilon \rho V V) = -\epsilon(\nabla P) + \nabla(\epsilon \tau) - \frac{\epsilon^2 \mu}{K} V \tag{4}$$

where ϵ is the porosity of the PTL; K the permeability of the medium. The momentum equation (4) for the porous media is written in terms of physical velocity, and simply adds a source term to the Navier–Stokes equation which approaches Darcy's law when the source term is dominant. With the inclusion of the inertia and the viscous terms, this equation is referred to as the Brinkmann–Forchheimer equation and it always differs from Darcy's law in that the higher-order terms in the viscous term require the use of a no-slip boundary condition at the solid walls that enclose the porous media. While the appropriateness of these additional terms is debatable [8], this equation is used in a regime that approaches the limiting case of Darcy's law.

In all cases, the flow is assumed to be steady with constant properties and the porous media are assumed to be isotropic.

4. Boundary conditions

The channel inlet and outlet boundaries are shown in Fig. 1. At the inlet, a constant velocity is specified corresponding to a given Reynolds number. The inlet velocity is assumed to be uniform across the cross-section. At the outlet, a constant pressure equal to atmospheric pressure is specified. A no-slip boundary condition is specified at the remaining boundaries. All the external boundaries of the porous transport block are assumed to be non-permeable.

5. Permeability values

By considering fully developed Poiseuille flow between parallel plates and equating the pressure drop to Darcy's law, the upper limit for permeability is given by:

$$K = \frac{H_p^2}{12} \tag{5}$$

where H_p is the thickness of the PTL. In our case, this corresponds to $K = 1.3 \times 10^{-10}\ m^2$ for a 40 μm PTL.

An excellent review of experimental permeability results for the fibrous materials that are typically used in PEM PTLs has been carried out by Jackson and James [9]. This paper presents non-dimensional permeability values as a function of the solid fraction ($\phi = 1 - \epsilon$) and shows that PTL permeabilities of the order of $10^{-10}\ m^2$ require fibre diameters of about 45 μm at a porosity of 0.7 (typical value for a PTL) with increases as the porosity decreases or as the desired permeability decreases. Clearly, a typical fibrous PTL is not appropriate for a micro-fuel cell where a direct scale-down suggests a PTL thickness of 30–40 μm. It is possible, however, to approach the limiting value of the permeability by designing a new PTL that is suitable for micro-fuel cells.

An alternative to a conventional PTL is an array of cylindrical micro wires connecting the flow-field plate to the catalyst region.

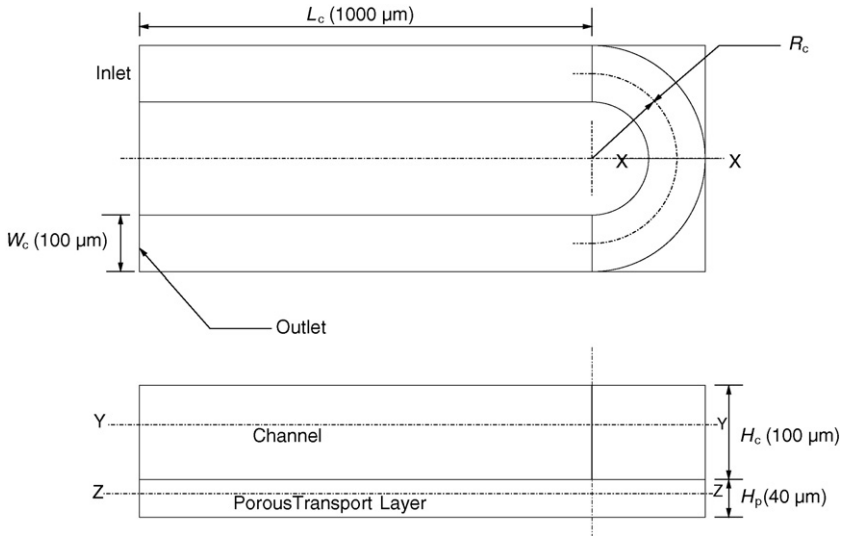

Fig. 1. Schematic of serpentine microchannel.

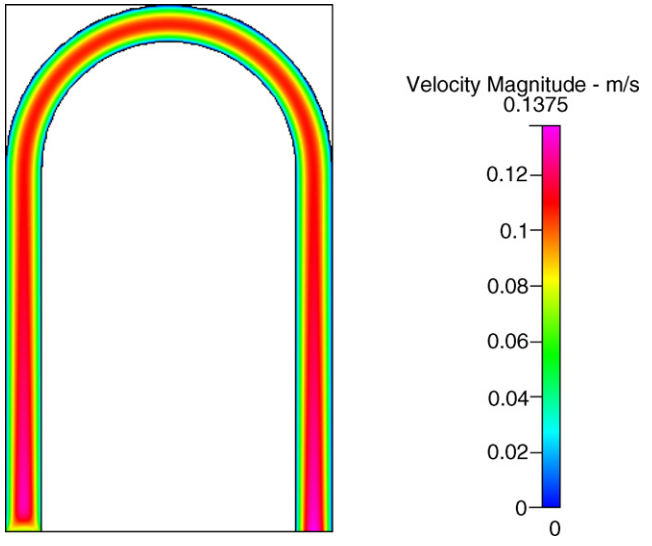

Fig. 2. Velocity profile in serpentine channel at section Y–Y for $Re = 0.45$, $\epsilon = 0.4$ and $K = 10^{-11}$ m^2.

The density and size of these micro wires can be set to obtain optimal fuel cell performance, and the desired permeability. The permeability of a regular array of cylinders is given in [9] as:

$$\frac{K}{a^2} = \frac{1}{8\phi}\left(-\ln\phi - \frac{3}{2} + 2\phi\right) \quad (6)$$

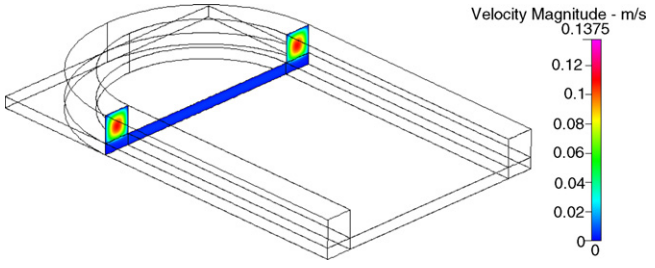

Fig. 3. Velocity profile before and after bend in serpentine channel for $Re = 0.45$, $\epsilon = 0.4$ and $K = 10^{-11}$ m^2.

where a is the cylinder radius. The equation can be used to estimate the radius required for a limiting permeability in the absence of sidewalls. This suggests that micro wire radii would have to be in the range of 12–38 μm at a porosity of 0.4 to maintain the permeability between 10^{-11} and 10^{-10} m^2.

6. Numerical simulation

The governing equations are solved using CFD-ACE+. The geometry is created and meshed using the CFD-GEOM modeller. The solution is obtained using CFD-ACE-SOLVER and the results are post-processed with CFD-VIEW. A combination of structured and unstructured grids is used. A grid independence study was carried out by successively refining the mesh. It is found that for number of cells equal to 447,420, any further refinement does not give an appreciable change in the solution. Hence, this mesh size is used in all the computations.

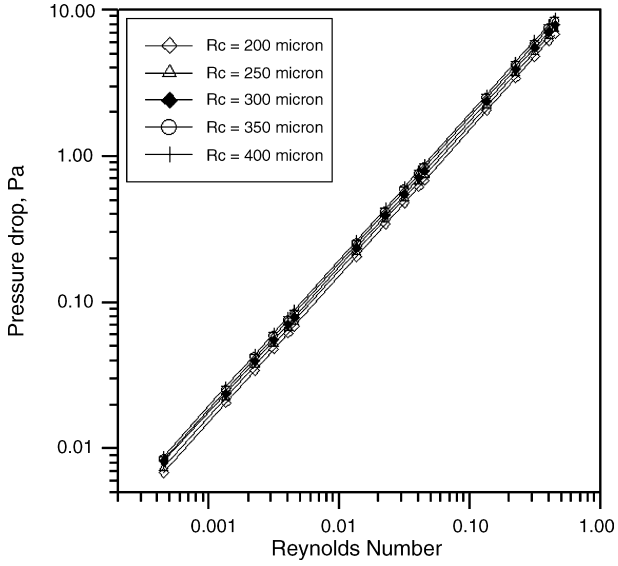

Fig. 4. Variation of pressure drop with Reynolds number for serpentine channel with PTL at $\epsilon = 0.4$ and $K = 10^{-11}$ m^2.

The Reynolds number is varied from 0.00045 to 0.45 and the permeability from 10^{-10} to 10^{-15} m^2.

7. Results and discussion

The surface plot of the velocity at section Y–Y, which is at the mid-plane along the channel thickness, is shown in Fig. 2. At some distance from the channel inlet, the velocity profile becomes fully developed. Fig. 3 shows this fully developed velocity profile at cross-sections before and after the bend. It is observed that the fully developed velocity profile continues up to the bend. The velocity profile in the presence of a PTL is slightly different compared with a fully developed velocity profile observed in a flow-through microchannel. At the bend, the velocity profile changes due to curvature of the channel. After the bend, the profile regains its fully developed nature in the straight segment of the channel.

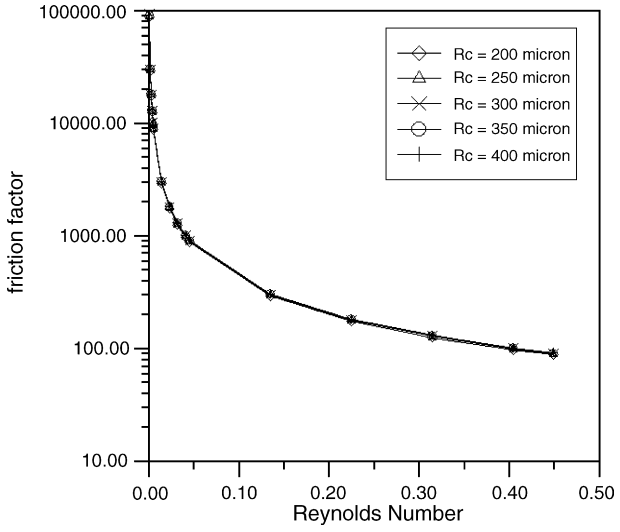

Fig. 5. Variation of friction factor with Reynolds number for serpentine channel with PTL at $\epsilon = 0.4$ and $K = 10^{-11}$ m^2.

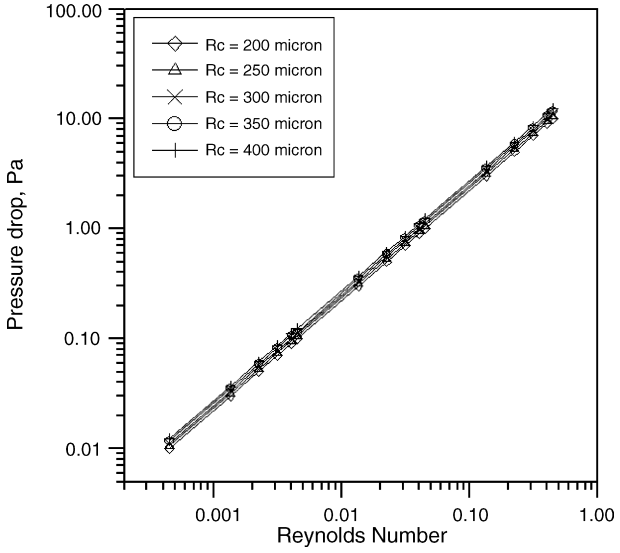

Fig. 6. Variation of pressure drop with Reynolds number for serpentine channel without PTL.

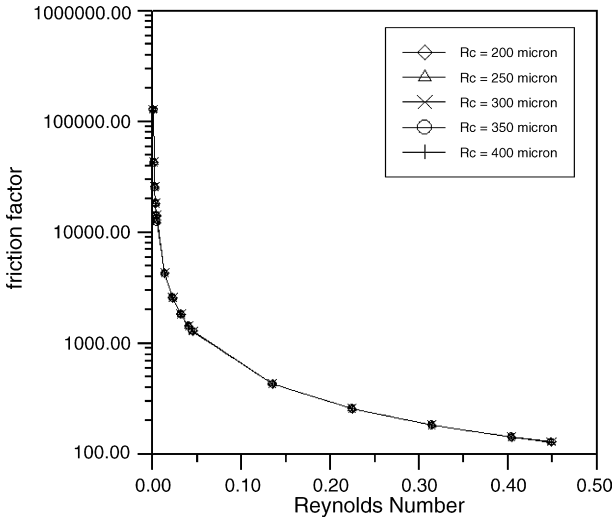

Fig. 7. Variation of friction factor with Reynolds number for serpentine channel without PTL.

The variation of pressure drop in the channel with Reynolds number is presented in Fig. 4 for channels with different values of radius of curvature R_c. Here, the Reynolds number is defined as:

$$Re = \frac{\rho V D_h}{\mu} \tag{7}$$

where D_h is the hydraulic diameter of the channel. It is observed that the pressure drop increases linearly with Reynolds number. For the same value of Reynolds number, the pressure drop increases with increase in the radius of curvature R_c. This is because, as R_c increases, the effective flow length also increases. Hence, more driving pressure is required for the flow to occur at

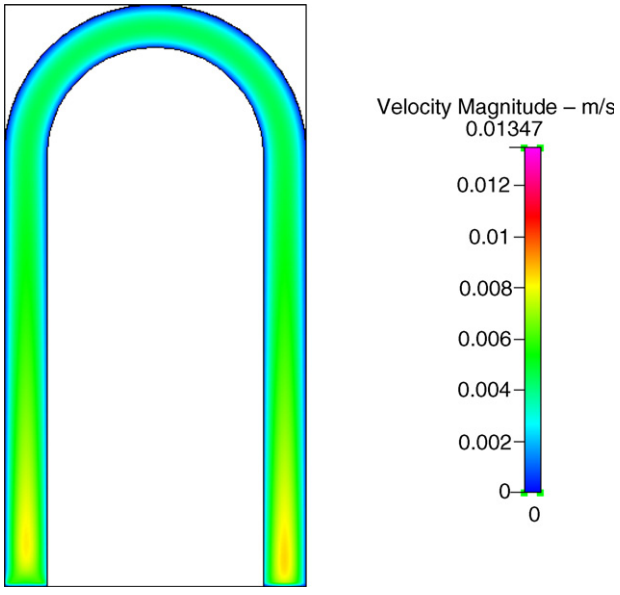

Fig. 8. Velocity profile at interface between serpentine channel and PTL for $Re = 0.314$, $\epsilon = 0.4$ and $K = 10^{-10}$ m^2.

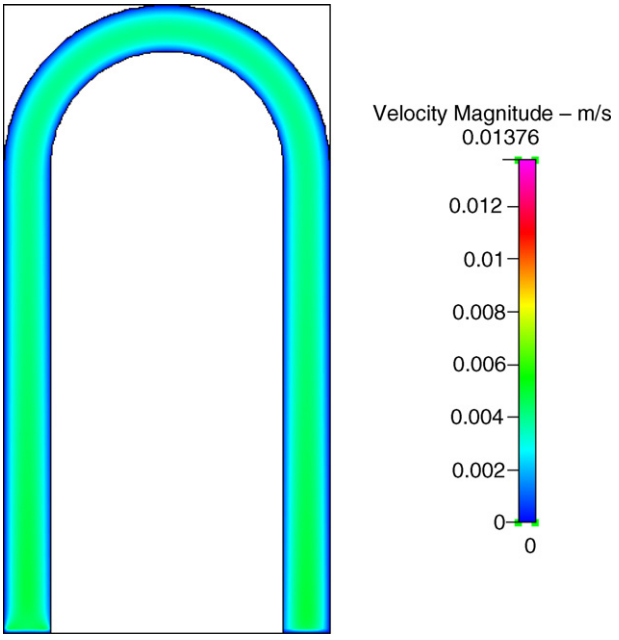

Fig. 9. Velocity profile at interface between serpentine channel and PTL for $Re = 0.314$, $\epsilon = 0.4$ and $K = 10^{-11}$ m^2.

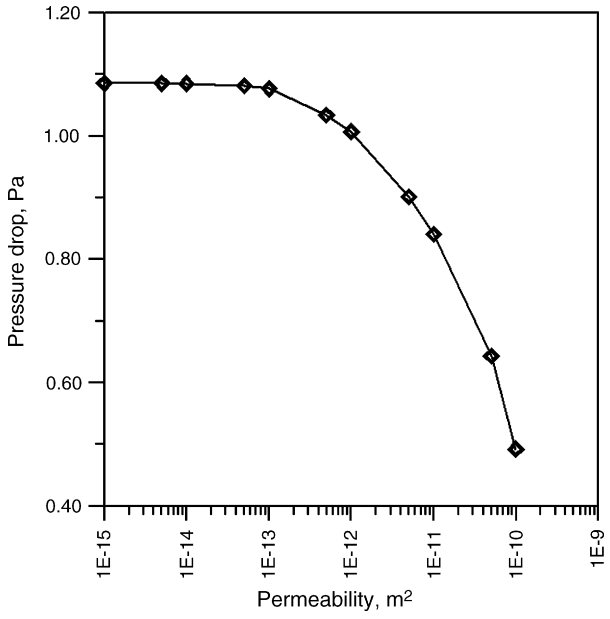

Fig. 11. Variation of pressure drop with permeability of PTL for serpentine channel at $Re = 0.045$, $R_c = 300$ μm and $\epsilon = 0.4$.

the same inlet velocity (i.e., same Reynolds number). A plot of friction factor against Reynolds number is given in Fig. 5. The friction factor is defined as:

$$f = \frac{\Delta P}{(1/2)\rho V^2}\frac{D_h}{L} \tag{8}$$

where $L = L_c + \pi R_c$ is the total flow length between channel inlet and outlet. The friction factor curves for different values of R_c collapse into single one, which indicates that the friction factor is independent of the radius of curvature for a given channel geometry. The variation in pressure drop and friction factor for a channel without PTL is shown in Figs. 6 and 7, respectively. The plots indicate that the variation of these parameters with Reynolds number is similar in nature to the flow through the channel with a PTL. The pressure drop and friction factor values are found to be lower for channels with PTLs. The presence of a transport layer increases the available area of flow in addition to the channel flow area. Hence, this results in lower pressure drop for channels with PTLs (Figs. 8–10).

The velocity magnitude along the interface between the microchannel and the PTL for three different permeability values of 10^{-10}, 10^{-11} and 10^{-12} m^2, respectively. It can be seen that the velocity increases with increase in permeability, which means

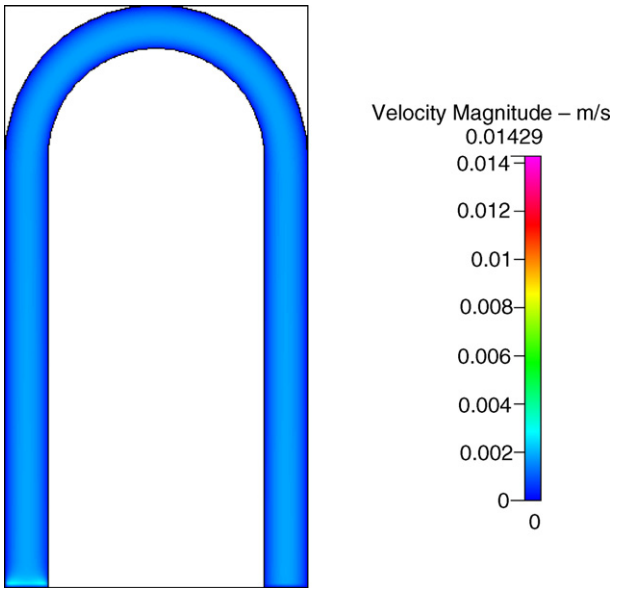

Fig. 10. Velocity profile at interface between serpentine channel and PTL for $Re = 0.314$ and $K = 10^{-12}$ m^2.

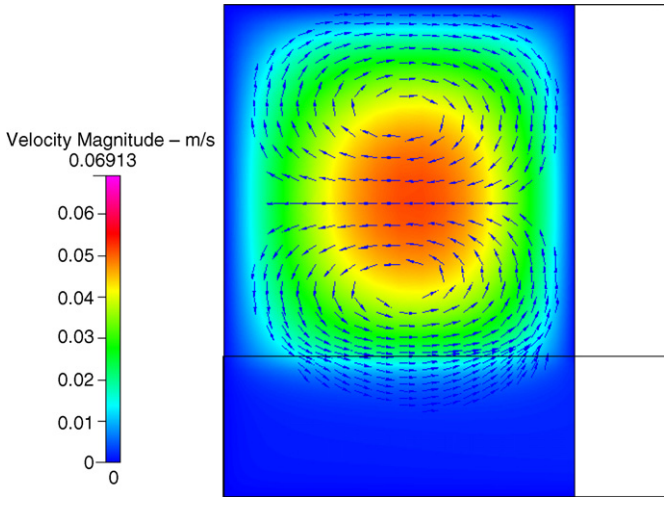

Fig. 12. Velocity magnitude and vector plot at bend (section X–X in Fig. 1) for $Re = 0.224$, $\epsilon = 0.4$ and $K = 10^{-10}$ m^2.

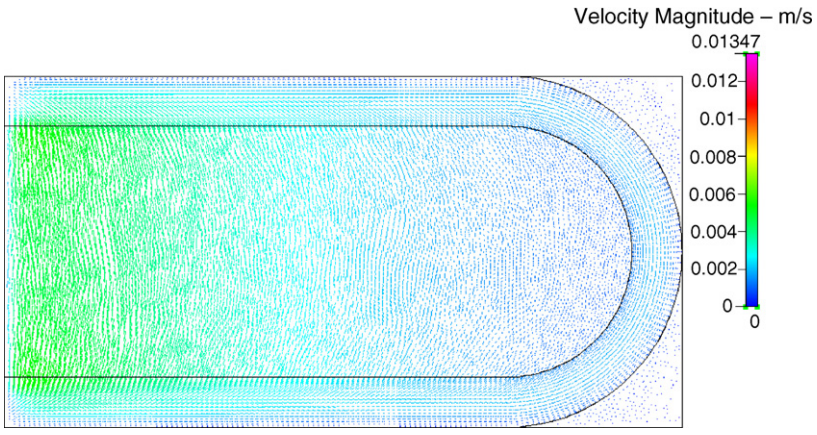

Fig. 13. Velocity vectors within PTL (section Z–Z Fig. 1) for $Re = 0.045$, $\epsilon = 0.4$ and $K = 10^{-10}\,m^2$.

more fluid flow occurs through the PTL, as the permeability is increased. At lower permeability, the PTL behaves as a solid plate, which is confirmed by a permeability value of $10^{-12}\,m^2$. The variation of pressure drop in the channel with the permeability of PTL is shown in Fig. 11. For a highly permeable PTL, the pressure drop is lower and increases as the permeability is decreased. It is found that there are two limits for the pressure drop and corresponding to two limiting values of permeability. The upper limit for the pressure drop is observed for a very low permeability value, which corresponds to the case of a micro-channel without a PTL (refer Fig. 6), while the lower limit is for a PTL with infinite permeability. In this case, the value of the lower limit is 0.38 Pa, which corresponds to a permeability value of $10^{-7}\,m^2$.

Fig. 12 shows the velocity at the centre of the bend for the section X–X (refer Fig. 1). It is found that a secondary flow pattern is present at the bend and is due to the centrifugal force acting on the fluid moving along the curved channel. The secondary flow is negligible at low Reynolds numbers. It becomes appreciable for Reynolds numbers in the range of 4×10^{-2} to 4.5×10^{-2}. This secondary flow is expected to cause additional pressure drop in case of serpentine channels compared with straight channels. A secondary flow, similar to this one, is also observed in serpentine channels without porous transport layers [6]. In the present case, however due to the presence of porous layer, the secondary flow vortices extend into the PTL, as shown in Fig. 12. This flow characteristic is quite different to the flow in a stand-alone micro-channel.

The velocity vectors at a cross-section along the half-thickness of the PTL (section Z–Z in Fig. 1) are shown in the Fig. 13. The serpentine micro-channel is over-layed on the figure to show the relative position of the channel with respect to the PTL. It is observed that the fluid flows through the PTL from the inlet to the exit section of the channel. Here, the fluid has two paths to travel between the inlet and the outlet of the channel. First, fluid flows along the length of the channel and, second, it passes underneath of the channel through the PTL. The fraction of fluid passing through the PTL reduces as the permeability is decreased. It is also observed that the magnitude of the velocity within the PTL is maximum close to the section that connects the inlet and the outlet, which corresponds to a maximum pressure gradient compared with other sections along the length of the channel.

8. Conclusions

A study has been made of convection through a microchannel with a porous transport layer, which is an integral component of a micro-PEMFC. It is found that the velocity profile in the channel becomes fully developed at some distance from the channel inlet, which is modified due to the porous layer. The pressure drop in the channel varies linearly with Reynolds number. At a particular Reynolds number, the pressure drop increases with increase in the radius of curvature. The variation of friction factor with Reynolds number indicates that the former is independent of the radius of curvature. The variations of pressure drop and friction factor in a channel without porous layer are similar in nature. On the other hand, the frictional loss for the channel in the absence of a PTL is greater than that for a channel with PTL. Fluid tends to flow through the PTL, bypassing the serpentine channel. The flow through the PTL increases as the permeability of the porous layer is increased. Hence, convection in micro-PEMFCs is modified by the inclusion of a PTL.

Acknowledgment

The support of the Suman Mashruwala μEngineering Laboratory, IIT Bombay is highly appreciated.

References

[1] J.G. Pharoah, J. Power Sources 144 (2005) 77–82.
[2] G.H. Guvelioglu, H.G. Stenger, J. Power Sources 147 (2005) 95–106.
[3] J. Ramousse, J. Deseure, O. Lottin, S. Didierjean, D. Maillet, J. Power Sources 145 (2005) 416–427.
[4] E. Hontanona, M. Escudero, C. Bautista, P.L. Garca-Ybarra, L. Daza, J. Power Sources 86 (2000) 363–368.

[5] A.S. Rawool, S.K. Mitra, A. Agrawal, S. Kandlikar, Numerical simulation of flow through microchannels in bipolar plate, Proceedings of Third International conference on Microchannels and Minichannels, Toronto, Canada, 2005.
[6] A. Rawool, S.K. Mitra, S.G. Kandlikar, Microfluidics and Nanofluidics 2 (2006) 215–221.
[7] S. Litster, J.G. Pharoah, G. McLean, N. Djilali, J. Power Sources 156 (2006) 334–344.
[8] D.A. Nield, A. Bejan, Convection in Porous Media, Springer-Verlag, Inc., NewYork, 1992.
[9] G.W. Jackson, D.F. James, Can. J. Chem. Eng. 64 (1986) 364–374.